



# Comparative study on the reliability of SnPbSb solder joint under common thermal cycling and extreme thermal shocking

Jianhao Wang<sup>1,2</sup> · Songbai Xue<sup>1</sup> · Jianxin Wang<sup>3</sup> · Peng Zhang<sup>1</sup> · Yu Tao<sup>1</sup> · Ziyi Wang<sup>1</sup>

Received: 12 January 2020 / Accepted: 16 February 2020 / Published online: 24 February 2020  
© Springer Science+Business Media, LLC, part of Springer Nature 2020

## Abstract

The increasingly severe temperature has always been a problem for the solder joint applied in the future novel electrical devices. The reliability evolution of solder joint in these conditions is necessary for the design of electrical packaging materials. In this paper, a common thermal cycling test of  $-65$  to  $150$  °C and an extreme thermal shocking test of  $-196$  to  $150$  °C were carried out on Sn50Pb49Sb1/Cu solder joint. The interfacial behavior of the solder joint, as well as the corresponding mechanical performance, was analyzed. In the thermal cycling test, the coarsening behavior of  $\text{Cu}_6\text{Sn}_5$  layer and the formation of a new  $\text{Cu}_3\text{Sn}$  layer were detected. After 400 cycles of thermal cycling, the shear force of solder joint was decreased by 31.55%, but the ductile fracture was hardly changed. The reliability of solder joint was more sensitive to the extreme thermal shocking. Besides the coarsening behavior of IMC layer, the micro-crack formation induced by thermal stress was obtained in  $\text{Cu}_6\text{Sn}_5$  layer. These micro-cracks became the crack source and gave a further decrement of the shear strength. After 400 cycles of extreme thermal shocking, the shear force of solder joint was reduced by 50.43%, giving a ductile/brittle mixed fracture.

## 1 Introduction

With the recent development of fifth generation (5G) cellular networks, the data transmission between electrical facilities has been unprecedentedly accelerated and higher power devices are being widely applied [1, 2]. Meanwhile, the electrical devices are gradually miniaturized owing to the advanced processing technology, giving a high integration level [3]. High-density integrated circuit greatly increased the portability of electrical products, but it also leads to a critical cooling problem for the electrical devices as well as their solder joints, especially for those applied in 5G cellular networks.

Solder joints, which provide the interconnection between electrical devices, are claimed to be sensitive to the periodic temperature change owing to the interfacial behavior [4–7]. Pang et al. [8] investigated the impact of  $-40$  to  $125$  °C thermal cycling on SnAgCu solder joint and found that after 1500 cycles of thermal cycling, a great deal of voids formed in the intermetallic compound (IMC) layer of solder joint, weakening the bond between solder matrix and Cu pad. Yang et al. [9] carried out a thermal cycling test ranging from  $-30$  to  $125$  °C on SnBi solder joint and not only the excessive growth of IMC layer but also the enrichment of brittle Bi phase in solder matrix was obtained after long-term thermal cycling, which gave a further decrease of strength. In the past decades, many efforts have been conducted to try to clarify the microstructure and performance evolution of solder joint in the common thermal cycling condition and it has been found that thermal cycling tests with different temperature profiles possessed different effects on solder joints [10]. Spelt et al. [11] conducted thermal cycling tests of  $0$ – $100$  °C and  $-40$  to  $125$  °C on the solder joint in the Plastic Ball Grid Array Package (PBGA), respectively, and found that the damage per cycles was increased with the temperature difference due to the higher thermal stress. Vries et al. [12] simulated the endurance behavior of solder joints subjected to two kinds of thermal cycle conditions ( $-40$  to  $125$  °C and

✉ Songbai Xue  
xuesb@nuaa.edu.cn

<sup>1</sup> College of Materials Science and Technology, Nanjing University of Aeronautics and Astronautics, Nanjing 210016, China

<sup>2</sup> Joining and Welding Research Institute (JWRI), Osaka University, Ibaraki, Osaka 567-0047, Japan

<sup>3</sup> Jiangsu Provincial Key Laboratory of Advanced Welding Technology, Jiangsu University of Science and Technology, Zhenjiang 212003, China

–55 to 125 °C) and found that the earlier fracture of solder joint was obtained in the latter condition. With the increasingly extensive application of electrical devices, solder joints are facing much more extreme temperature conditions, such as cosmic and polar environments [13]. For example, the low-earth-orbit (LEO) satellite would be exposed to a severe temperature ranging from –170 to 123 °C, which gave the solder joint an extreme thermal shocking [14]. But currently the investigations on the effect of extreme thermal shocking on solder joint are rarely reported. Therefore, to comprehend the reliability difference between solder joints subjected to various extreme temperature conditions, the comparative investigation on the microstructure and property evolution of solder joint under common thermal cycling and extreme thermal shocking is necessary.

Pb-containing solder alloys, which although have been prohibited in the commercial electrical products, are still widely used in the martial and astronautical equipment due to their excellent wettability and cryogenic property [15]. In comparison with eutectic SnPb solder alloy, Sn50Pb50 solder with higher resistance to thermal load is preferred in the electrical system applied in the aerospace industry. The trace addition of Sb element was found to be able to enhance the reliability of solder joint subjected to thermal cycling [16]. Hence SnPbSb solder alloy is seen as an excellent packaging material for the future novel electrical devices for aerospace industry. In this article, Sn50Pb49Sb1 solder joint was exposed to a common thermal cycling of –65 to 150 °C and an extreme thermal shocking of –196 to 150 °C, respectively. The interfacial microstructure and mechanical properties evolution of solder joint in the two conditions were analyzed and compared to provide reference for the future investigation on solder alloy applied in the extreme conditions.

## 2 Experimental

Sn50Pb49Sb1 solder alloy was made by high-purity metals of Sn, Pb, and Sb and then soldered on Cu pads at 250 °C to prepare the samples. The experiment parameters of the common thermal cycling (TC) and the extreme thermal shocking (TS) are listed in Table 1. The thermal cycling test was conducted in a thermal cycling test chamber according to American Military Standard MIL-STD-883 and the maximum/minimum temperatures were 150 °C/–65 °C. The dwell time was 20 min and the ramp rate of temperature was nearly 15 °C/min. The extreme thermal shocking test was provided by liquid Nitrogen (–196 °C) and a constant temperature chamber which was set as 150 °C. The dwell period was also 20 min and the ramp rate of temperature was too difficult to be measured as the exchanging process between maximum/minimum temperature was finished immediately. After 0,

**Table 1** The experiment parameters of TC and TS test

	TC test	TS test
Maximum temperature (°C)	150	150
Minimum temperature (°C)	–65	–196
Dwell time (min)	20	20
Ramp rate of temperature (°C/min)	Nearly 15	Hard to be obtained

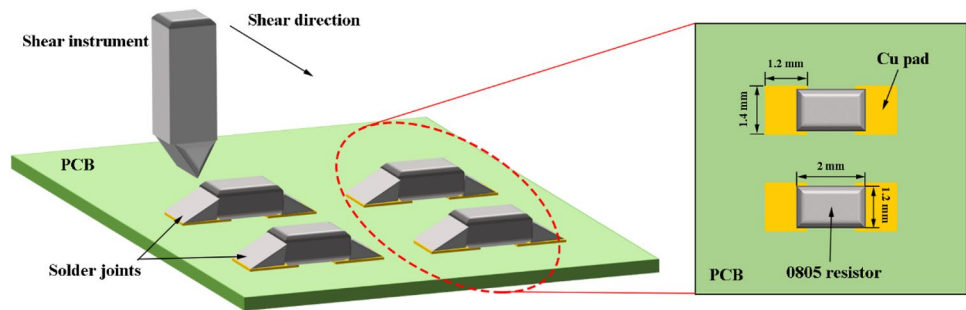
200, 400 cycles of TC and TS test, part of samples were taken out to be analyzed.

After TC and TS test, these samples were divided into two groups, where one is for cross-sectional observation and the other is for top-view observation. The samples in cross-sectional observation group were cut and polished to analyze the effect of TC or TS on the cross-sectional IMC morphology. The samples in top-view observation group were deeply etched by a mixed solution of 13 ml HNO<sub>3</sub> and 87 ml H<sub>2</sub>O with continuous ultrasonic concussion and then cleaned by ethyl alcohol to remove all solder matrix and provide a top-view observation on the IMC layer. The microstructure was analyzed by the scanning electron microscope (SEM) and the energy-dispersive spectrometer (EDS).

The strength test of solder joint was conducted in accordance with Japanese Industrial Standard JIS Z 3198-7. 0805 resistors were soldered on the printed circuit board by the prepared Sn50Pb49Sb1 solder in advance and then subjected to the TC and TS test. After every 100 cycles, 10 resistors were tested by an STR-1000 joint strength tester, as shown in Fig. 1. The shear instrument of strength tester was set in front of the resistor and then moved at 2 mm/min along the shear direction to push the resistor and break the solder joint. The maximum shear force during the test process was taken to assess the strength evolution of solder joint and the fracture observation was also carried out to clarify the fracture characteristics.

## 3 Results and discussion

The interfacial layer growth under thermal load was always a serious problem for the solder joint due to the high brittleness of IMC [17, 18]. Figure 2 exhibits the cross-sectional SEM images of SnPbSb/Cu solder joint after different cycles of TC and TS tests. It could be seen from Fig. 2 that after soldering process, a scallop-like Cu<sub>6</sub>Sn<sub>5</sub> IMC layer formed at the interface of solder matrix and Cu pad, which indicated that the solder matrix was bonded well with Cu [19]. But with the increasing cycles, Cu<sub>6</sub>Sn<sub>5</sub> layers in solder joints were subjected to TC and TS tests; both thickened and their morphologies were changed to be flatter and flatter. Moreover, the formation of new Cu<sub>3</sub>Sn layer between Cu<sub>6</sub>Sn<sub>5</sub> layer

**Fig. 1** The diagram of shear test

Cycles	Thermal cycling	Thermal shocking
0		
200		
400		

**Fig. 2** The cross-sectional microstructure of interfacial layer in solder joint at different parameters

and Cu pad could be obtained in both conditions, which gave an extensive growth of interfacial layer. It could be seen from Fig. 2 that at the same cycles of TC and TS test, the total thicknesses of IMC layers in two conditions were quite similar, but the  $\text{Cu}_6\text{Sn}_5$  layer of solder joint subjected to TS test showed some different behaviors. After 400 TC cycles, the  $\text{Cu}_6\text{Sn}_5$  layer of solder joint thickened significantly and kept a holonomic morphology without any obvious defects. Whereas after being subjected to 400 TS cycles, many micro-cracks formed in the  $\text{Cu}_6\text{Sn}_5$  layer, which gave a broken morphology. Some  $\text{Cu}_6\text{Sn}_5$  particles were tending to lose the reliable bond with IMC layer.

Figure 3 shows the top-view images of solder joint during TC and TS tests and Table 2 lists the corresponding EDS results. As shown in Fig. 3a, the interfacial layer surface of as-soldered joint was rough and the magnified image in Fig. 3b indicated the surface of the IMC layer with hill-like morphology with ravines. This IMC layer was identified to be  $\text{Cu}_6\text{Sn}_5$  IMC, which was consistent with the cross-sectional observation. After 400 TC cycles, the surface of  $\text{Cu}_6\text{Sn}_5$  layer was changed to be much flatter and the original ravines were filled up, as shown in Fig. 3c and d. The same phenomenon was observed in solder joint after 400 TS cycles, where the flattening behavior of  $\text{Cu}_6\text{Sn}_5$  layer was also obtained. But it was interesting to find that a few new hollows formed at the surface, which were not detected in the TC samples. The corresponding magnified image in Fig. 3f indicated that at the bottom of these hollows, there were some broken grains which were identified to be  $\text{Cu}_6\text{Sn}_5$  IMC. It could be concluded that some  $\text{Cu}_6\text{Sn}_5$

grains were broken during the TS test and were removed in the following deep etching process, exhibiting a fragmentary morphology. As  $\text{Cu}_3\text{Sn}$  layer was at the interface between  $\text{Cu}_6\text{Sn}_5$  layer and Cu, it was too hard to detect  $\text{Cu}_3\text{Sn}$  layer in the top-view observation.

The microstructure evolution of IMC layer during TC and TS test could be attributed to the atomic migration under thermal load [20]. The growth behavior of interfacial layers was a migration-dominant process which was greatly accelerated at the high-temperature stage of TC and TS tests [21]. The increasing cycles gave a high Cu content at the interface and hence gradually coarsening  $\text{Cu}_6\text{Sn}_5$  layer was obtained. Moreover, once the Cu content exceeded the threshold, the original  $\text{Cu}_6\text{Sn}_5$  would transform to  $\text{Cu}_3\text{Sn}$  IMC, which started from the interface between  $\text{Cu}_6\text{Sn}_5$  and Cu. Therefore, coarsening bilayer structure was obtained in both TC and TS tests. But the coarsening IMC layer with high brittleness has been claimed to be adverse to the reliability of solder joint [22]. In the temperature-changing condition, the coefficient of thermal expansion (CTE) difference between solder matrix and Cu pad made the interface a stress-concentration area and increased the probability of cracks formation, especially for the wide temperature range of TS test. Therefore, the stress intensity factor  $K_I$  at the interface was increased during the TC and TS process and once  $K_I$  exceeded  $K_{IC}$ , which was the fracture toughness of IMC layer, the formation and prolongation of cracks were obtained [23]. Pang et al. [8] reported that the  $K_{IC}$  value of  $\text{Cu}_3\text{Sn}$  without defects was higher than that of  $\text{Cu}_6\text{Sn}_5$ , which gave  $\text{Cu}_6\text{Sn}_5$  a higher fracture risk under stress. In the cross-sectional observation, no defects were detected in the  $\text{Cu}_3\text{Sn}$  layer of solder joint during TS test and hence micro-cracks occurred in  $\text{Cu}_6\text{Sn}_5$  layer rather than  $\text{Cu}_3\text{Sn}$  after 400 TS cycles [24]. But in comparison to the TS test, no cracks were observed in the solder joint subjected to the TC test. This was consistent with previous researches and may be ascribed to the low temperature range of TC test, where the  $K_I$  of IMC layer during TC test was lower than  $K_{IC}$  [25, 26]. The formation of micro-cracks in TS test destroyed the reliable bonding between  $\text{Cu}_6\text{Sn}_5$  grains, giving a broken morphology. As a result, the detached  $\text{Cu}_6\text{Sn}_5$  grains

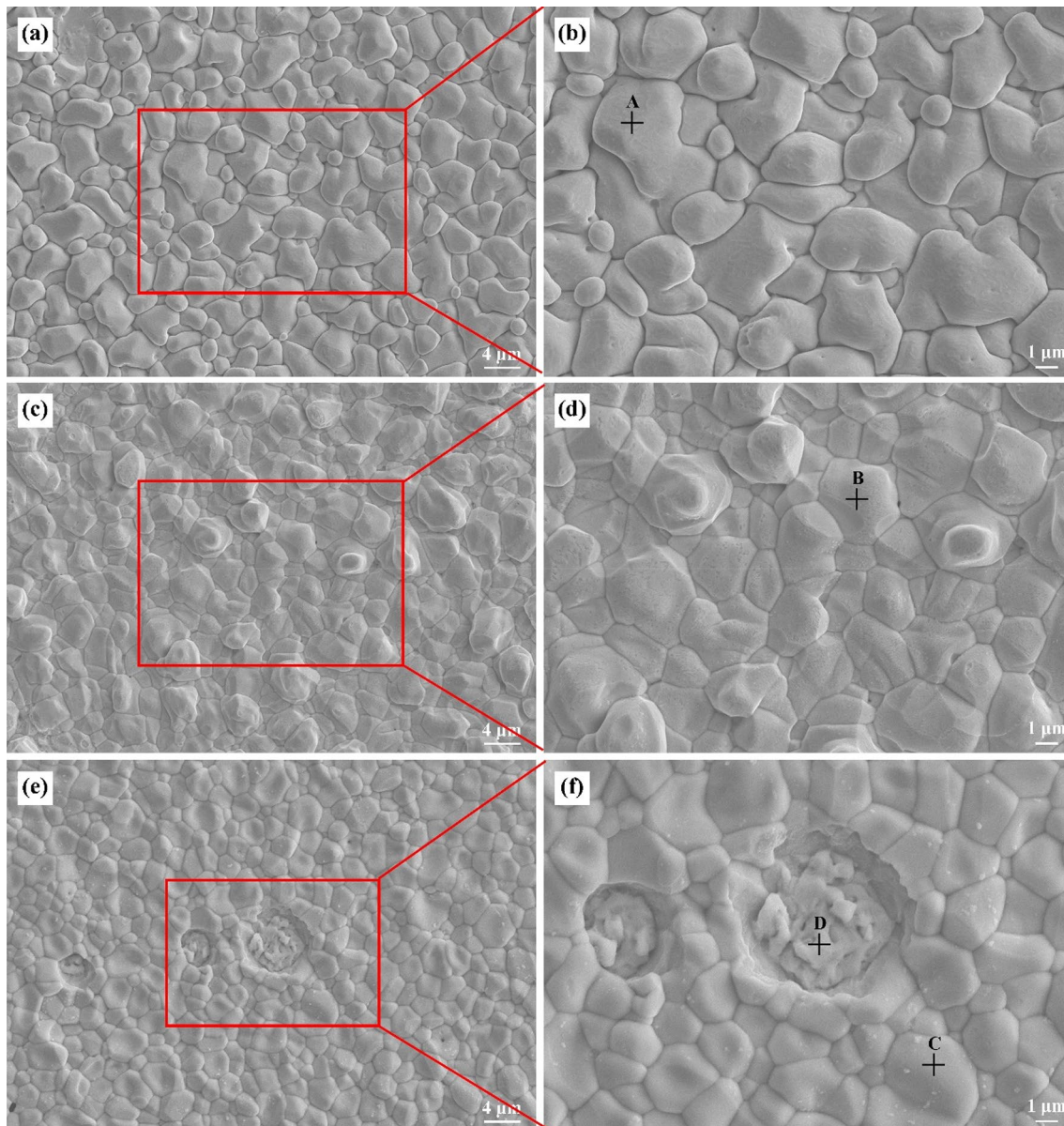


**Fig. 3** The top-view SEM images of solder joints in various conditions. **a** as-soldered solder joint and **b** its high-magnification image; **c** solder joint after 400 TC cycles and **d** its high-magnification image; **e** solder joint after 400 TS cycles and **f** its high-magnification image

**Table 2** The EDS results of Fig. 3

Points	Composition (at.%)	
	Cu	Sn
A	52.27	47.73
B	54.59	45.41
C	56.17	43.83
D	55.63	44.37

from IMC layer in cross-sectional observation and the broken  $\text{Cu}_6\text{Sn}_5$  grains in top-view observation were obtained.

The strength of solder joint was claimed to be significantly affected by the behavior of IMC layer [27, 28]. Figure 4 shows the shear force evolution of SnPbSb/Cu solder joint during the TS and TC test. The solder matrix and Cu pad were bonded well in the as-soldered joint, which gave a shear force of 51.12 N. With the increasing cycles, the shear forces of solder joint subjected to TC and TS test were both reduced gradually, but the downtrend in TS test was more obvious than that in TC test. After 400 cycles, the shear force of solder joint was decreased by 50.43% for TS test,

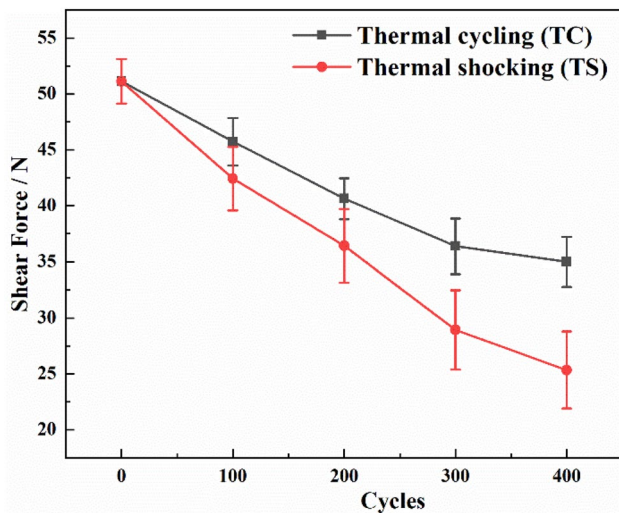


**Fig. 4** The shear force of solder joint during the TC and TS test

while 31.55% for TC test. It could be concluded that at the same cycle, the effect of extreme thermal shocking on the strength of solder joint was much more serious than that of common thermal cycling. The excessive growth of brittle  $\text{Cu}_6\text{Sn}_5$  and  $\text{Cu}_3\text{Sn}$  layers resulted in the deteriorating strength of solder joint during TC and TS tests [29, 30]. The CTE mismatch of solder matrix and Cu pad made the brittle interfacial layer become the stress-concentration area, which led to the fracture of solder joint at the relatively low stress level in the shear test. Hence the increasing cycles deteriorated the shear force of solder joint. Moreover, as shown in Figs. 2 and 3, although the IMC thicknesses of solder joint in TS and TC test were similar, the broken behavior of  $\text{Cu}_6\text{Sn}_5$  layer with the formation of micro-cracks during TS test provided the crack sources in the solder joint, which promoted the initiation and prolongation of cracks in the shear test [31]. Therefore, the micro-cracks induced by extreme thermal stress gave a further decline of shear force during the TS test.

To clarify the fracture characteristics of solder joint during the TC and TS test, the fracture analysis was conducted in this section. Figure 5 exhibited the fracture images of SnPbSb/Cu solder joint at different cycles of TC or TS test, as well as the corresponding elemental mapping results. As shown in Fig. 5a, a great number of shear dimples formed on the fracture surface of as-soldered joint and no characteristics of brittle fracture were obtained. Moreover, the corresponding elemental mapping in Fig. 5b detected high content of Sn, Pb, and Sb at the fracture surface, where the content of Cu element was negligible. It could be concluded that for the as-soldered joint, the ductile fracture occurred in the solder matrix during the shear test [32, 33]. After 400 TC cycles, the morphology of solder joint still consisted of shear dimples and compared to the as-soldered joint, the Cu

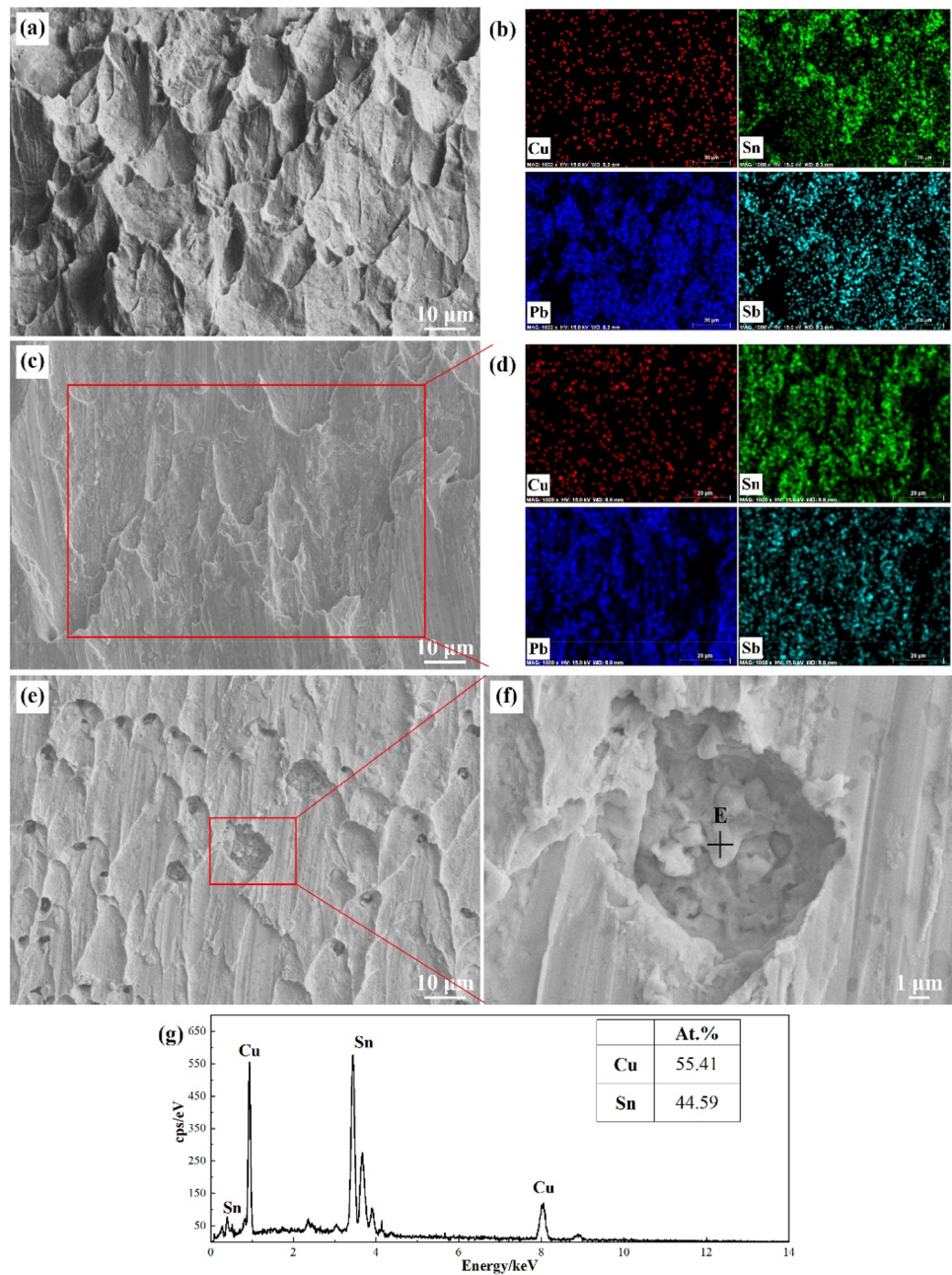
content was slightly increased, as illustrated in Fig. 5c and d. This phenomenon indicated that although the fracture mode of solder joint was still ductile fracture, the fracture position was changed to the solder matrix near the interface [34]. However, the fracture morphology of solder joint after 400 TS cycles was quite different from the former two, as exhibited in Fig. 5e. Although the majority of fracture surface was still shear dimples in solder matrix, there were many hollows at the bottom of dimples. The high-magnification image in Fig. 5f exhibited the morphology of dimple with the hollow. At the bottom of these hollows, there were some broken grains, which showed brittle fracture characteristics. These broken grains were clarified to be  $\text{Cu}_6\text{Sn}_5$  by EDS analysis, as shown in Fig. 5g. For the solder joint subjected to 400 TS cycles, the fracture during shear test initiated at the  $\text{Cu}_6\text{Sn}_5$  layer and prolonged in the nearby solder matrix, giving a ductile/brittle mixed fracture mode.

Usually, Sn-based solder matrix possessed lower strength than brittle IMC layer and the fracture of as-soldered joint occurred in the ductile solder matrix [35]. Hence as shown in Fig. 5a and b, the fracture morphology of as-soldered joint exhibited the ductile dimples of solder matrix. However, with the increasing TC cycles, the growth of brittle IMC layer and the accumulation of thermal stress which was induced by the CTE mismatch weakened the interface area [17]. At this time, the fracture resistance of IMC layer was still higher than solder matrix and hence the fracture of solder joint after 400 TC cycles occurred in the solder matrix near the interface, showing the ductile dimples [26]. But the micro-cracks in  $\text{Cu}_6\text{Sn}_5$  layer induced by TS test, provided the crack sources and significantly deteriorated the IMC layer [36]. Therefore, the fracture of solder joint after 400 TS cycles initiated in the brittle  $\text{Cu}_6\text{Sn}_5$  layer and prolonged in the nearby solder matrix, exposing the broken  $\text{Cu}_6\text{Sn}_5$  grains at the bottom of dimples.

## 4 Conclusion

In this paper, the effect of common thermal cycling and extreme thermal shocking on the interfacial layer and mechanical property of SnPbSb/Cu solder joint was studied contrastively. The results indicated that the thicknesses of IMC layer in two conditions were quite similar at the same cycles due to the growth behavior of IMC, but the harmful effect of extreme thermal shocking was more serious than that of thermal cycling. After 400 TS cycles, many micro-cracks formed in the  $\text{Cu}_6\text{Sn}_5$  layer, which showed a broken morphology in the cross-sectional and top-view observation, deteriorating the strength. After 400 cycles of TC and TS test, the shear forces of solder joint were reduced by 31.55% and 50.43%, respectively. After 400 TC cycles, the ductile fracture of solder joint

**Fig. 5** The fracture morphology of solder joint at different parameters. **a** As-soldered solder joint and **b** its elemental mapping; **c** solder joint after 400 TC cycles and **d** its elemental mapping; **e** solder joint after 400 TS cycles and **f** its high-magnification image; **g** the EDS result of point E



was hardly changed, but the fracture position was transformed to solder matrix near the interface. But for the solder joint after TS test, the fracture initiated in the broken  $\text{Cu}_6\text{Sn}_5$  layer and then prolonged in the nearby solder matrix, which showed ductile/brittle mixed fracture characteristics.

**Acknowledgements** This research was supported by the National Natural Science Foundation of China (Grant No. 51675269); Nanjing University of Aeronautics and Astronautics PhD short-term visiting scholar project (Grant No. 190908DF06); and Priority Academic Program Development of Jiangsu Higher Education Institutions (PAPD).

## References

1. L. Dai, B. Wang, Y. Yuan, S. Han, I. Chin-Lin, Z. Wang, *IEEE Commun. Mag.* **53**, 74 (2015)
2. S. He, R. Gao, J. Li, Y.-A. Shen, H. Nishikawa, *Mater. Chem. Phys.* **239**, 122309 (2020)
3. Y.-A. Shen, S. Zhou, J. Li, C.-H. Yang, S. Huang, S.-K. Lin, H. Nishikawa, *Mater. Des.* **183**, 108144 (2019)
4. A. Sharma, Y.-J. Jang, J.B. Kim, J.P. Jung, *J. Alloys Compd.* **704**, 795 (2017)
5. J. Wu, S. Xue, J. Wang, P. Xue, *J. Electron. Mater.* **48**, 4562 (2019)
6. Y. Zuo, L. Ma, S. Liu, T. Wang, F. Guo, X. Wang, *J. Mater. Sci.* **48**, 2318 (2013)

7. S. He, R. Gao, Y.-A. Shen, J. Li, H. Nishikawa, J. Mater. Sci. **55**, 3107 (2020)
8. L. Xu, J.H.L. Pang, F. Che, J. Electron. Mater. **37**, 880 (2008)
9. L. Yang, L. Zhu, Y. Zhang, S. Zhou, G. Wang, S. Shen, X. Shi, Mater. Charact. **148**, 280 (2019)
10. M. Dusek, Solder. Surf. Mount Technol. **17**, 22 (2005)
11. Y. Qi, R. Lam, H.R. Ghorbani, P. Snugovsky, J.K. Spelt, Microelectron. Reliab. **46**, 574 (2006)
12. J.W.C. de Vries, M.Y. Jansen, W.D. van Driel, Microelectron. Reliab. **47**, 444 (2007)
13. J. Wang, S. Xue, P. Zhang, P. Zhai, Y. Tao, J. Mater. Sci. Mater. Electron. **30**, 9065 (2019)
14. G. Pippin, Prog. Org. Coat. **47**, 424 (2003)
15. J. Wang, S. Xue, Z. Lv, L. Wen, S. Liu, Appl. Sci. **8**, 1706 (2018)
16. Y. Zhong, W. Liu, C. Wang, X. Zhao, J.F. Caers, Mater. Sci. Eng. A **652**, 264 (2016)
17. H.-T. Lee, M.-H. Chen, H.-M. Jao, T.-L. Liao, Mater. Sci. Eng. A **358**, 134 (2003)
18. J. Wang, S. Xue, P. Zhang, Z. Wang, P. Zhai, J. Mater. Sci. Mater. Electron. **31**, 1421 (2020)
19. Y.-A. Shen, C.-M. Lin, J. Li, S. He, H. Nishikawa, Sci. Rep. **9**, 3658 (2019)
20. Y.-A. Shen, C.-M. Lin, J. Li, R. Gao, H. Nishikawa, Sci. Rep. **9**, 10210 (2019)
21. H. Wang, S. Xue, J. Wang, J. Mater. Sci. Mater. Electron. **28**, 8246 (2017)
22. H. Nishikawa, N. Iwata, J. Mater. Process. Technol. **215**, 6 (2015)
23. V.L. Nguyen, C.-S. Chung, H.-K. Kim, Microelectron. Reliab. **55**, 2808 (2015)
24. O. Minho, G. Vakanas, N. Moelans, M. Kajihara, W. Zhang, Microelectron. Eng. **120**, 133 (2014)
25. J.W.R. Teo, Y.F. Sun, Acta Mater. **56**, 242 (2008)
26. J. Wang, S. Xue, Z. Lv, L. Wen, S. Liu, J. Mater. Sci. Mater. Electron. **30**, 4990 (2019)
27. F.X. Che, J.H.L. Pang, J. Alloys Compd. **541**, 6 (2012)
28. Y.D. Han, H.Y. Jing, S.M.L. Nai, L.Y. Xu, C.M. Tan, J. Wei, Intermetallics **31**, 72 (2012)
29. Y.H. Lee, H.T. Lee, Mater Sci Eng A **444**, 75 (2007)
30. C. Hang, R. Tian, L. Zhao, Y. Tian, Appl. Sci. **8**, 2056 (2018)
31. R. Tian, C. Hang, Y. Tian, J. Feng, J. Alloys Compd. **777**, 463 (2019)
32. J. Wang, S. Xue, Z. Lv, L. Wang, H. Liu, L. Wen, J. Mater. Sci. Mater. Electron. **29**, 20726 (2018)
33. J. Wang, H. Nishikawa, Microelectron. Reliab. **54**, 1583 (2014)
34. X. Li, F. Li, F. Guo, Y. Shi, J. Electron. Mater. **40**, 51 (2011)
35. Y. Tian, C. Hang, C. Wang, S. Yang, P. Lin, Mater. Sci. Eng. A **529**, 468 (2011)
36. R. Tian, C. Hang, Y. Tian, L. Zhao, Mater. Sci. Eng. A **709**, 125 (2018)

**Publisher's Note** Springer Nature remains neutral with regard to jurisdictional claims in published maps and institutional affiliations.